CHAPTER 7

INVESTIGATION ON THERMOELASTIC BEHAVIOR OF A FUNCTIONALLY GRADED SPHERICAL SHELL UNDER HEAT CONDUCTION MODEL WITH A DELAY[1]

7.1 Introduction

The basic structural elements like plate, disk, cylinder, sphere, etc. have practical applications in engineering design problems and the expected loads play very critical role in designing such structural elements. The concept of functionally graded materials (FGMs) is originated in Japan in 1984 during the space plane project in the form of a proposed thermal barrier material that is capable of withstanding a surface temperature of 2000 K and a temperature gradient of 1000K across a cross section $<$ 10mm. Thereafter, an extensive research on FGMs are being persuaded to understand their proper utility in realistic sense as compared to composite materials. The functionally graded materials (FGMs) are now considered as new advanced heat resisting materials used in modern technologies due to their potential to carry ultra high thermal stresses. Furthermore, these materials are corrosion and erosion resistant and have high fracture stiffness. The basic concept in such materials is to mix different materials (for

[1]The content of this chapter is ***communicated*** **to an** ***International Journal***, **2018**.

example ceramic and metal) such that the material properties continuously vary from one constituent material to the other. In effect, the material properties are coordinate dependent, as they are treated as functions of position.

A great interest is being paid during last two decades to analyze the responses of FGMs under different applied mechanical and thermal loads. However, since the governing equations for the temperature field and the associated thermoelastic field become nonlinear, it is difficult to obtain the exact solutions. In order to solve the thermoelastic problems of FGM approximately, introducing the theory of laminated composites is efficient. Several studies (see Tanigawa(1995), Ootao *et al.* (1995) and Tanigawa *et al.* (1996) and references therein) have been proposed to analyze the transient thermoelastic problems of FGMs by using the theory of laminated composites. Tanigawa obtained the closed-form solutions of problems with the steady-state condition for the heat conduction problems and analyzed thermal stresses that occur in a structure made of non-homogeneous materials. Obata and Noda (1994; 1995) investigated the thermal stresses in a functionally graded circular hollow cylinder and sphere by using the perturbation method. Solution for stresses in spheres made of functionally graded materials is discussed by Lutz and Zimmerman (1996). Zimmerman and Lutz (1999) obtained the exact solution for the problem of uniformly heating cylinder by considering the case when the elastic moduli and thermal expansion coefficient vary linearly with radius. Later on, Shabana and Noda (2001) investigated the thermoelastoplastic stresses in a full functionally graded plate subjected to a thermal load. Sankar and

Tzeng (2002) obtained the axial stress distribution for a FGM beam by solving the thermoelastic equilibrium equations. It must be mentioned that Liew *et al.* (2003) analyzed the thermal stress behavior of FGM hollow circular cylinders. Here, the solutions are obtained by a novel limiting process that employs the solutions of homogeneous hollow circular cylinders, with no recourse to the basic theory or the equations of non-homogeneous thermoelasticity. Here, conclusions are made regarding the general properties of thermal stresses in the FGM cylinder. Reddy and Chin (1998) reported a thermo-mechanical analysis of FGM cylinders and plates. Darabseh and Bani Salameh (2010) used classical heat conduction model to investigate the transient thermal stresses in a FGM cylinder with different thermal boundary conditions. They have employed a numerical method based on implicit finite difference scheme to calculate the temperature, radial displacement and stress distributions within the cylinder. Bakhshi *et al.* (2006) studied the response of FG hollow disk based on the classical theory of thermoelasticity under thermal shock loads. We also refer a recent book by Hetnarski and Eslami (2008) in this respect. By considering FGMs in generalized thermoelasticity theories, Ghosh and Kanoria (2008; 2009), Mallik and Kanoria (2007), Banik and Kanoria (2013), Hosseini (2009) reported some investigations. Bahtui and Eslami (2007a; 2007b) investigated the coupled thermoelasticity and generalized coupled thermoelasticity of FG cylindrical shells subjected to thermal shock, respectively. Later on, the response of a FG disk is studied by Bagri and Eslami (2008) under the LS theory. Hein *et al.* (2012) made a comparison of the temperature and stresses obtained by finite difference method

and finite element method. Recently, Kothari and Mukhopadhyay (2013) studied a problem of functionally graded hollow disk under three phase-lag and dual-phase-lag thermoelasticity theories. Zhang *et al.* (2013) tackled the non-linearity of the thermoelasticty problem generated by FGM using Green's function approach.

In the previous chapter, we studied a problem of non-homogeneous thermoelastic medium by considering the temperature dependent material properties of the medium. In the present chapter, we make an attempt to investigate a problem of spherical shell with functionally graded material in the context of the recent heat conduction model (Quintanilla, 2011). We employ Galerkin type finite element method along with Laplace transform technique to solve a system of non-linear coupled partial differential equations arising out in the coupled problem. We consider a metal-ceramic FGM by assuming that the inner boundary of the shell is stress free and is subjected to thermal shock while the other boundary is insulated with temperature and fixed with some rigid support. We consider a law of mixture of material constituents so that the effective material properties follow a rule of volume-fraction. We show that the present problem can be solved by trans-finite element method, i.e., firstly, we use the Laplace transform technique to remove the dependency of governing equations on time. Then, in order to tackle the non-linearity of governing equations generated due to dependency of thermal parameters on spacial coordinate, we apply finite element method by considering that the geometry of the shell is divided into discrete elements of equal length along the radius of the shell. We carry out our computational work in MATLAB programming code and ob-

tain the numerical solution of the problem. The results are displayed in different graphs to display the distributions of the field variables inside the shell at different time and for various types of non-homogeneity condition. A detailed comparative study on the obtained results is discussed to focus on the functionally graded material and the effect of non-homogeneity. The present work specially considers to highlight the necessity of the finite element method to tackle the problems on coupled thermoelasticity for functionally graded materials and to display a comparative analysis of the results under present model and the same under other different coupled thermoelasticity theories.

7.2 Formulation of the Problem

We consider a spherical shell of functionally graded materials (FGMs) constituent with metal and ceramic. The effective material properties of FGMs are generally defined by a relation that exhibits the effective material properties of the FGM to the constituent material properties. It is assumed that the composition of the metal and ceramic is followed by a law of mixture of material constituents and the effective material properties of FGM are defined as

$$P = V_m(P_m - P_c) + P_c \tag{7.1}$$

where V_m is the volume fraction of the metal, P is the effective property of FGM and the subscripts m and c indicate the metal and ceramic features, respectively. Therefore, P_m and P_c denote the properties of metal and

ceramic, respectively.

7.2.1 Basic Governing Equations

The basic governing equations in the context of the different generalized thermoelastic theories incorporated for a non-homogeneous medium in absence of any body force or heat source is given by the following relations:

Equation of motion:

$$\sigma_{ij,j} = \rho \ddot{u}_i \tag{7.2}$$

Stress-strain-temperature relation:

$$\sigma_{ij} = 2\mu e_{ij} + (\lambda e_{kk} - \gamma\theta)\,\delta_{ij} \tag{7.3}$$

Strain displacement relation:

$$2e_{ij} = u_{i,j} + u_{j,i} \tag{7.4}$$

From Eqns. (7.2) and (7.3), we get

$$\left[2\mu e_{ij} + (\lambda e_{kk} - \gamma\theta)\,\delta_{ij}\right]_{,j} = \rho \ddot{u}_i \tag{7.5}$$

We consider an unified heat conduction equation as

$$\begin{aligned}\left(\delta_{2z} + \delta_{1z}\frac{\partial}{\partial t}\right)(K\theta_{,i})_{,i} + \left(1 + \tau_1\frac{\partial}{\partial t} + z_1\frac{\tau_1^2}{2}\frac{\partial^2}{\partial t^2}\right)(K^*\theta_{,i})_{,i} \\ = \left(1 + \tau_0\frac{\partial}{\partial t}\right)\left(\delta_{2z} + \delta_{1z}\frac{\partial}{\partial t}\right)\left[\rho c_E\frac{\partial\theta}{\partial t} + T_0\gamma\frac{\partial e}{\partial t}\right]\end{aligned} \tag{7.6}$$

where, K and K^* are the thermal conductivity and conductivity rate, respectively. $\eta = \frac{\rho c_E}{K}$ and c_E is the specific heat at constant strain. τ and

τ_0 are the delay parameter/thermal relaxation parameter. The material properties, except the thermal relaxation parameters or delay term, which appeared in the preceding equations (7.2)–(7.6) for the FGMs are the effective material properties and are treated as position dependent functions.

In order to analyze our results in the present context with the corresponding results in the contexts of some generalized thermoelastic models namely, Lord-Shulman theory (LS Model), Green-Naghdi thermoelasticity theory of type-II (GN-II Model) and thermoelasticity theory given by Quintanilla (New model), we consider a unified heat conduction equation given by Eqn. (7.6). The individual heat conduction equation for different theories can be extracted from Eqn. (7.6) by assuming the values of parameter constants as follows:

(i). **LS Model (Lord and Shulman (1967)):** $z = 2$, $\tau_0 > 0$ and $K^* = 0$

(ii). **GN-II Model (Green and Naghdi (1993)):** $z = 1$, $\tau_1 = 0$, $\tau_0 = 0$ and $K = 0$

(iii). **New Model (Quintanilla (2011)):** $z = 1$, $z_1 = 1$, $\tau_0 = 0$ and $\tau > 0$

In the context of present problem, we take a thermoelastic functionally graded spherical shell at rest and reference temperature T_0. The inner radius and outer radius of the shell are assumed to be r_a and r_b, respectively. Considering radially symmetric motion, the only non-zero component of the displacement is the radial displacement component u. Hence, the two non-zero strain components are

$$e_{rr} = \frac{\partial u}{\partial r}; \quad e_{\phi\phi} = \frac{u}{r}. \tag{7.7}$$

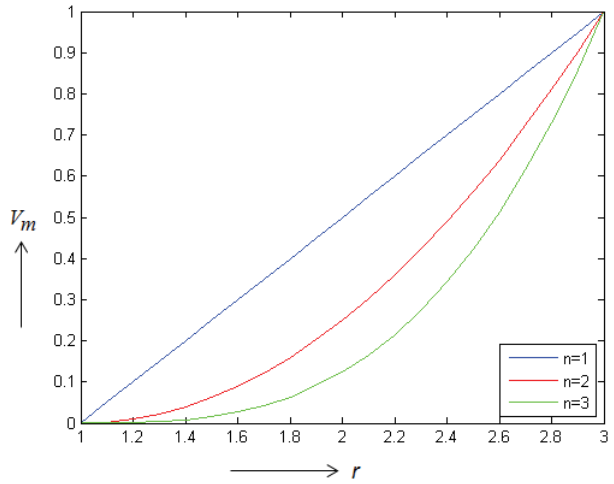

Figure 7.1: Variation of volume fraction of the constituents of functionally graded material

Therefore, Eqns. (7.2)-(7.3) and (7.5)-(7.6) reduce to the following forms:

$$\frac{\partial \sigma_{rr}}{\partial r} + \frac{2\left(\sigma_{rr} - \sigma_{\phi\phi}\right)}{r} = \rho \frac{\partial^2 u}{\partial t^2} \tag{7.8}$$

$$\sigma_{rr} = 2\mu \frac{\partial u}{\partial r} + \lambda \left(\frac{\partial u}{\partial r} + \frac{2u}{r} \right) - \gamma\theta \tag{7.9}$$

$$\sigma_{\varphi\varphi} = 2\mu \frac{u}{r} + \lambda \left(\frac{\partial u}{\partial r} + \frac{2u}{r} \right) - \gamma\theta \tag{7.10}$$

$$(\lambda + 2\mu) \left[\frac{\partial^2 u}{\partial r^2} + \frac{2}{r}\frac{\partial u}{\partial r} - \frac{2u}{r^2} \right] + \frac{\partial\left(\lambda + 2\mu\right)}{\partial r}\frac{\partial u}{\partial r} + \frac{2u}{r}\frac{\partial \lambda}{\partial r} - \left[\gamma \frac{\partial \theta}{\partial r} + \frac{\partial \gamma}{\partial r}\theta \right] = \rho \frac{\partial^2 u}{\partial t^2} \tag{7.11}$$

$$\begin{aligned} &\left[K\left(\delta_{2z} + \delta_{1z}\frac{\partial}{\partial t} \right) + K^*\left(1 + \tau_1 \frac{\partial}{\partial t} + z_1 \frac{\tau_1^2}{2}\frac{\partial^2}{\partial t^2} \right) \right] \left(\frac{\partial^2 \theta}{\partial r^2} + \frac{2}{r}\frac{\partial \theta}{\partial r} \right) \\ &\quad + \left[\frac{\partial K}{\partial r}\left(\delta_{2z} + \delta_{1z}\frac{\partial}{\partial t} \right) + \frac{\partial K^*}{\partial r}\left(1 + \tau_1 \frac{\partial}{\partial t} + z_1 \frac{\tau_1^2}{2}\frac{\partial^2}{\partial t^2} \right) \right] \frac{\partial \theta}{\partial r} \\ &\quad = \left(1 + \tau_0 \frac{\partial}{\partial t} \right) \left(\delta_{2z} + \delta_{1z}\frac{\partial}{\partial t} \right) \left[\rho c_E \frac{\partial \theta}{\partial t} + T_0 \gamma \frac{\partial}{\partial t}\left(\frac{\partial u}{\partial r} + \frac{2u}{r} \right) \right] \end{aligned} \tag{7.12}$$

Further, we assume material composition in the functionally graded shell

along the radial direction in such a manner that the inner surface and outer surface of the shell are made of ceramic and metal, respectively and the gradual change in composition of the constituent materials in the radial direction is assumed to vary in the form of the law

$V_m = \left(\frac{r-r_a}{r_b-r_a}\right)^n$

where r is the radial coordinate and n is the non-homogeneity index that govern the distribution of the constituent materials through the shell (as shown in Fig. (7.1)). Here, the non-homogeneity index, n may be varied to obtain different profiles for the distribution of constituent materials. Clearly, the present composition indicates that the effective properties of shell are followed by metal in the case when n $\to 0$, and they are followed by ceramic, when $n \to \infty$

Now, to simplify the problem, we introduce the following non-dimensional parameters and notations:

$r' = c_0\eta_0 r$, $\theta' = \frac{\theta}{T_d}$, $(t', \tau_0', \tau_1') = c_0^2\eta_0\,(t, \tau_0, \tau_1)$, $u' = \frac{c_0\eta_0(\lambda_m+2\mu_m)}{\gamma_m T_d}u$,
$\left(\sigma_{rr}', \sigma_{\varphi\varphi}'\right) = \frac{(\sigma_{rr},\sigma_{\varphi\varphi})}{\gamma_m T_d}$, $c_0^2 = \frac{(\lambda_m+2\mu_m)}{\rho_m}$, $\eta_0 = \frac{\rho_m c_m}{K_m}$.

where T_d is a dimensionless characteristic temperature.

Using the above parameters and notations and dropping the primes for convenience Eqns. (7.9)-(7.12) take the following forms:

$$\sigma_{rr} = \frac{2\mu}{(\lambda_m+2\mu_m)}\frac{\partial u}{\partial r} + \frac{\lambda}{(\lambda_m+2\mu_m)}\left(\frac{\partial u}{\partial r} + \frac{2u}{r}\right) - \frac{\gamma}{\gamma_m}\theta \qquad (7.13)$$

$$\sigma_{\varphi\varphi} = \frac{2\mu}{(\lambda_m+2\mu_m)}\frac{u}{r} + \frac{\lambda}{(\lambda_m+2\mu_m)}\left(\frac{\partial u}{\partial r} + \frac{2u}{r}\right) - \frac{\gamma}{\gamma_m}\theta \qquad (7.14)$$

$$\frac{(\lambda+2\mu)}{(\lambda_m+2\mu_m)}\left[\frac{\partial^2 u}{\partial r^2}+\frac{2}{r}\frac{\partial u}{\partial r}-\frac{2u}{r^2}\right]+\frac{1}{(\lambda_m+2\mu_m)}\frac{\partial\left(\lambda+2\mu\right)}{\partial r}\frac{\partial u}{\partial r}$$
$$+\frac{1}{(\lambda_m+2\mu_m)}\frac{2u}{r}\frac{\partial\lambda}{\partial r}-\frac{1}{\beta_m}\left[\gamma\frac{\partial\theta}{\partial r}+\frac{\partial\gamma}{\partial r}\theta\right]=\frac{\rho}{\rho_m}\frac{\partial^2 u}{\partial t^2} \tag{7.15}$$

$$\left[\frac{K}{K_m}\left(\delta_{2z}+\delta_{1z}\frac{\partial}{\partial t}\right)+\frac{K^*}{a_0}\left(1+\tau_1\frac{\partial}{\partial t}+z_1\frac{\tau_1^2}{2}\frac{\partial^2}{\partial t^2}\right)\right]\left(\frac{\partial^2\theta}{\partial r^2}+\frac{2}{r}\frac{\partial\theta}{\partial r}\right)$$
$$+\left[\frac{1}{K_m}\left(\delta_{2z}+\delta_{1z}\frac{\partial}{\partial t}\right)\frac{\partial K}{\partial r}+\frac{1}{a_0}\left(1+\tau_1\frac{\partial}{\partial t}+z_1\frac{\tau_1^2}{2}\frac{\partial^2}{\partial t^2}\right)\frac{\partial K^*}{\partial r}\right]\frac{\partial\theta}{\partial r}$$
$$=\left(1+\tau_0\frac{\partial}{\partial t}\right)\left(\delta_{2z}+\delta_{1z}\frac{\partial}{\partial t}\right)\left[\frac{\rho c_E}{\rho_m c_{Em}}\frac{\partial\theta}{\partial t}+\frac{\epsilon\gamma}{\gamma_m}\frac{\partial}{\partial t}\left(\frac{\partial u}{\partial r}+\frac{2u}{r}\right)\right] \tag{7.16}$$

where $a_0=c_0^2\eta_0 K_m$ and $\epsilon=\frac{T_0\gamma_m^2}{\rho_m c_m(\lambda_m+2\mu_m)}$.

7.2.2 Boundary Conditions

We assume that the inner surface of the spherical shell is assumed stress free but exposed to a thermal shock while the outer surface is rigidly fixed and thermally insulated. The mechanical and thermal boundary conditions at the inner and outer surfaces of the shell are therefore defined as

$$\left.\begin{array}{c}\theta\left(a,t\right)=\theta^* H(t),\ \ \sigma_{rr}(a,t)=0.\\ \frac{\partial\theta}{\partial r}\left(b,t\right)=0,\ \ u(b,t)=0.\end{array}\right\} \tag{7.17}$$

7.3 Solution using Galerkin Finite Element Method

Applying the Laplace transform to Eqns. (7.13)-(7.17), the equations transform to the following forms:

$$\overline{\sigma}_{rr} = \frac{2\mu}{(\lambda_m + 2\mu_m)}\frac{\partial \overline{u}}{\partial r} + \frac{\lambda}{(\lambda_m + 2\mu_m)}\left(\frac{\partial \overline{u}}{\partial r} + \frac{2\overline{u}}{r}\right) - \frac{\gamma}{\gamma_m}\overline{\theta} \tag{7.18}$$

$$\overline{\sigma}_{\varphi\varphi} = \frac{2\mu}{(\lambda_m + 2\mu_m)}\frac{\overline{u}}{r} + \frac{\lambda}{(\lambda_m + 2\mu_m)}\left(\frac{\partial \overline{u}}{\partial r} + \frac{2\overline{u}}{r}\right) - \frac{\gamma}{\gamma_m}\overline{\theta} \tag{7.19}$$

$$\begin{aligned}\frac{(\lambda + 2\mu)}{(\lambda_m + 2\mu_m)}\left[\frac{\partial^2 \overline{u}}{\partial r^2} + \frac{2}{r}\frac{\partial \overline{u}}{\partial r} - \frac{2\overline{u}}{r^2}\right] + \frac{1}{(\lambda_m + 2\mu_m)}\frac{\partial\left(\lambda + 2\mu\right)}{\partial r}\frac{\partial \overline{u}}{\partial r} \\ + \frac{1}{(\lambda_m + 2\mu_m)}\frac{2\overline{u}}{r}\frac{\partial \lambda}{\partial r} - \frac{1}{\gamma_m}\left[\gamma\frac{\partial \overline{\theta}}{\partial r} + \frac{\partial \gamma}{\partial r}\overline{\theta}\right] = \frac{\rho s^2}{\rho_m}\overline{u}\end{aligned} \tag{7.20}$$

$$\begin{aligned}&\left[\frac{K}{K_m}\left(\delta_{2z} + s\delta_{1z}\right) + \frac{K^*}{a_0}\left(1 + \tau_1 s + z_1\frac{\tau_1^2 s^2}{2}\right)\right]\left(\frac{\partial^2 \overline{\theta}}{\partial r^2} + \frac{2}{r}\frac{\partial \overline{\theta}}{\partial r}\right) \\ &\quad + \left[\frac{\left(\delta_{2z} + s\delta_{1z}\right)}{K_m}\frac{\partial K}{\partial r} + \frac{1}{a_0}\left(1 + \tau_1 s + z_1\frac{\tau_1^2 s^2}{2}\right)\frac{\partial K^*}{\partial r}\right]\frac{\partial \overline{\theta}}{\partial r} \\ &\quad = \left(1 + \tau_0 s\right)\left(\delta_{2z} + \delta_{1z}s\right)\left[\frac{\rho c_E s}{\rho_m c_{Em}}\overline{\theta} + \frac{\epsilon\gamma s}{\gamma_m}\left(\frac{\partial \overline{u}}{\partial r} + \frac{2\overline{u}}{r}\right)\right]\end{aligned} \tag{7.21}$$

$$\left.\begin{aligned}\overline{\theta}\left(a, s\right) = \tfrac{\theta^*}{s}, \;\; \overline{\sigma}_{rr}(a, s) = 0. \\ \tfrac{\partial \overline{\theta}}{\partial r}\left(b, s\right) = 0, \;\; \overline{u}(b, s) = 0.\end{aligned}\right\} \tag{7.22}$$

Now, we employ finite element method to solve the coupled Eqns. (7.20) and (7.21). For this, the geometry of the shell is divided into M discrete elements of equal length, h along the radius of the shell. Considering the base element as e_l, $(l = 1, 2, ...M)$, the displacement and temperature fields over the base element are approximated as

$$\overline{u}^{e_l} = \sum_{i=1}^{d} N_i^{e_l} \overline{U}_i^{e_l} \text{ and } \overline{\theta}^{e_l} = \sum_{i=1}^{d} N_i^{e_l} \overline{\theta}_i^{e_l} \tag{7.23}$$

where the $N_i^{e_l}$ denotes the shape function that approximates the displacement and temperature fields in the base element and d is the number of nodes in the base element. $\overline{U}_i^{e_l}$ and $\overline{\theta}_i^{e_l}$ $(i = 1, 2, ..., d)$ are therefore the nodal values of displacement and temperature, respectively. The arrangement of elements are shown in Fig. (7.2).

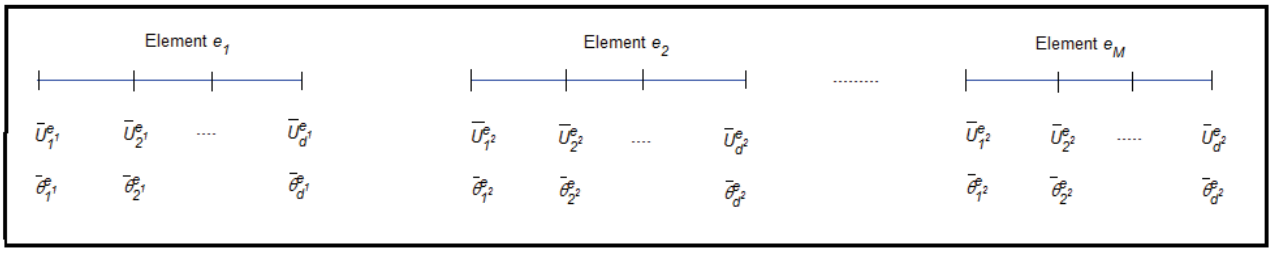

Figure 7.2: Graphical representation of base elements and nodes of finite element method

Employing the approximated fields for the displacement and temperature in the base element (e_l) and applying the Galerkin finite element method over the volume of the base element $V_{(e)}$, Eqns. (7.20) and (7.21) yield

$$\int_{V_{e_l}} \left[\frac{(\lambda + 2\mu)}{(\lambda_m + 2\mu_m)} \left(\frac{\partial^2 \overline{u}^{e_l}}{\partial r^2} + \frac{2}{r} \frac{\partial \overline{u}^{e_l}}{\partial r} - \frac{2\overline{u}^{e_l}}{r^2} \right) + \frac{1}{(\lambda_m + 2\mu_m)} \frac{\partial (\lambda + 2\mu)}{\partial r} \frac{\partial \overline{u}^{e_l}}{\partial r} + \frac{2}{r (\lambda_m + 2\mu_m)} \frac{\partial \lambda}{\partial r} \overline{u}^{e_l} \right.$$
$$\left. - \frac{\rho s^2}{\rho_m} \overline{u}^{e_l} \right] N_i^{e_l} dV_{e_l} - \int_{V_e} \left[\frac{1}{\gamma_m} \left(\gamma \frac{\partial \overline{\theta}^{e_l}}{\partial r} + \frac{\partial \gamma}{\partial r} \overline{\theta}^{e_l} \right) \right] N_i^{e_l} dV_{e_l} = 0 \tag{7.24}$$

$$
\begin{aligned}
&- \int_{V_e} \left[\left\{ (1+\tau_0 s)\left(\delta_{2z}+\delta_{1z}s\right) \frac{\epsilon\gamma s}{\gamma_m} \left(\frac{\partial \overline{u}^{e_l}}{\partial r} + \frac{2\overline{u}^{e_l}}{r} \right) \right\} \right] N_i^{e_l} dV_{e_l} \\
&+ \int_{V_{e_l}} \left[\left\{ \frac{K}{K_m}\left(\delta_{2z}+s\delta_{1z}\right) + \frac{K^*}{a_0}\left(1+\tau_1 s + z_1 \frac{\tau_1^2 s^2}{2}\right) \right\} \left(\frac{\partial^2 \overline{\theta}^{e_l}}{\partial r^2} + \frac{2}{r}\frac{\partial \overline{\theta}^{e_l}}{\partial r} \right) \right. \\
&\quad + \left\{ \frac{\left(\delta_{2z}+s\delta_{1z}\right)}{K_m}\frac{\partial K}{\partial r} + \frac{1}{a_0}\frac{\partial K^*}{\partial r}\left(1+\tau_1 s + z_1\frac{\tau_1^2 s^2}{2}\right) \right\} \frac{\partial \overline{\theta}^{e_l}}{\partial r} \\
&\quad \left. - (1+\tau_0 s)\left(\delta_{2z}+\delta_{1z}s\right)\frac{\rho c_E s}{\rho_m c_{Em}}\overline{\theta}^{e_l} \right] N_i^{e_l} dV_{e_l} = 0 \qquad (7.25)
\end{aligned}
$$

where $i = 1, 2, ..., d$.

Now, the weak formulation is applied to the terms involving the derivatives of the second order to lower their orders and to extract mixed boundary conditions with respect to the radial variable. Using the local coordinates $\xi = r - r_l$, where r_l is the radius of the first node of the base element, (e_l) in radial direction and using $dV_{e_l} = rdr = (\xi + r_l)\, d\xi$, Eqns. (7.24) and (7.25) reduce to the following equations:

$$
\begin{aligned}
&\int_0^h \left[\frac{(\lambda+2\mu)}{(\lambda_m+2\mu_m)}\left(\xi+r_i\right)^2 \frac{\partial N_i^{e_l}}{\partial \xi}\frac{\partial \overline{u}^{e_l}}{\partial \xi} + \left\{ \frac{(\lambda+2\mu)}{(\lambda_m+2\mu_m)} - \frac{2\left(\xi+r_i\right)}{(\lambda_m+2\mu_m)}\frac{\partial \lambda}{\partial \xi} + \frac{\rho s^2}{\rho_m}\left(\xi+r_i\right)^2 \right\} N_i^{e_l}\overline{u}^{e_l} \right] d\xi \\
&\quad + \int_0^h \frac{1}{\gamma_m}\left[\gamma \frac{\partial \overline{\theta}^{e_l}}{\partial \xi} + \frac{\partial \gamma}{\partial \xi}\overline{\theta}^{e_l} \right] \left(\xi+r_i\right)^2 N_i^{e_l} d\xi = \left[\frac{(\lambda+2\mu)}{(\lambda_m+2\mu_m)}\left(\xi+r_i\right)^2 N_i^{e_l}\frac{\partial \overline{u}^{e_l}}{\partial \xi} \right]_0^h \qquad (7.26)
\end{aligned}
$$

$$
\begin{aligned}
&\int_0^h (1+\tau_0 s)\left(\delta_{2z}+\delta_{1z}s\right)\frac{s\gamma\epsilon}{\gamma_m}\left[\left(\xi+r_i\right)\frac{\partial \overline{u}^{e_l}}{\partial \xi} + \overline{u}^{e_l} \right] \left(\xi+r_i\right) N_i^{e_l} d\xi + \int_0^h \left[\left\{ \frac{K}{K_m}\left(\delta_{2z}+s\delta_{1z}\right) \right. \right. \\
&\left. \left. + \frac{K^*}{a_0}\left(1+\tau_1 s + z_1\frac{\tau_1^2 s^2}{2}\right) \right\} \left(\xi+r_i\right)^2 \frac{\partial N_i^{e_l}}{\partial \xi}\frac{\partial \overline{\theta}^{e_l}}{\partial \xi} + (1+\tau_0 s)\left(\delta_{2z}+\delta_{1z}s\right)\frac{\rho c_E s}{\rho_m c_{Em}}\left(\xi+r_i\right)^2 N_i^{e_l}\overline{\theta}^{e_l} \right] d\xi \\
&\quad = \left[\left\{ \frac{K}{K_m}\left(\delta_{2z}+s\delta_{1z}\right) + \frac{K^*}{a_0}\left(1+\tau_1 s + z_1\frac{\tau_1^2 s^2}{2}\right) \right\} \left(\xi+r_i\right)^2 N_i^{e_l}\frac{\partial \overline{\theta}^{e_l}}{\partial \xi} \right]_0^h \qquad (7.27)
\end{aligned}
$$

Here h is the length of the base element (e_l) along the radius.

Using eqn. (7.23) into the Eqns. (7.26) and (7.27), we can form the finite element formulation in the Laplace transform domain as

$$\begin{bmatrix} [P^{e_l}] & [Q^{e_l}] \\ [R^{e_l}] & [S^{e_l}] \end{bmatrix} \begin{bmatrix} [\overline{U}^{e_l}] \\ [\overline{\theta}^{e_l}] \end{bmatrix} = \begin{bmatrix} [F^{e_l}] \\ [G^{e_l}] \end{bmatrix} \tag{7.28}$$

where the sub-matrices $\left[P^{e_l}\right]$, $\left[Q^{e_l}\right]$, $\left[R^{e_l}\right]$, $\left[S^{e_l}\right]$, each of order $(d \times d)$ and $\left[F^{e_l}\right]$, $\left[G^{e_l}\right]$, each of order $(d \times 1)$, defined for the base element (e_l) are obtained as follows:

$$P_{ij}^{e_l} = \int_0^h \left[\frac{(\lambda + 2\mu)}{(\lambda_m + 2\mu_m)} (\xi + r_i)^2 \frac{\partial N_i^{e_l}}{\partial \xi} \frac{\partial N_j^{e_l}}{\partial \xi} + \left\{ \frac{(\lambda + 2\mu)}{(\lambda_m + 2\mu_m)} - \frac{2(\xi + r_i)}{(\lambda_m + 2\mu_m)} \frac{\partial \lambda}{\partial \xi} + \frac{\rho s^2}{\rho_m} (\xi + r_i)^2 \right\} N_i^{e_l} N_j^{e_l} \right] d\xi \tag{7.29}$$

$$Q_{ij}^{e_l} = \int_0^h \frac{1}{\gamma_m} \left[\gamma \frac{\partial N_j^{e_l}}{\partial \xi} + \frac{\partial \gamma}{\partial \xi} N_j^{e_l} \right] (\xi + r_i)^2 N_i^{e_l} d\xi \tag{7.30}$$

$$R_{ij}^{e_l} = (1 + \tau_0 s)(\delta_{2z} + \delta_{1z} s) \frac{s^2 \epsilon}{\gamma_m} \int_0^h \gamma \left[(\xi + r_i) \frac{\partial N_j^{e_l}}{\partial \xi} + N_j^{e_l} \right] (\xi + r_i) N_i^{e_l} d\xi \tag{7.31}$$

$$S_{ij}^{e_l} = \int_0^h \left[\left\{ \frac{K}{K_m} (\delta_{2z} + s\delta_{1z}) + \frac{K^*}{a_0} \left(1 + \tau_1 s + z_1 \frac{\tau_1^2 s^2}{2} \right) \right\} \frac{\partial N_i^{e_l}}{\partial \xi} \frac{\partial N_j^{e_l}}{\partial \xi} + (1 + \tau_0 s)(\delta_{2z} + \delta_{1z} s) \frac{\rho c_E s}{\rho_m c_{Em}} N_i^{e_l} N_j^{e_l} \right] (\xi + r_i)^2 d\xi \tag{7.32}$$

$$F_i^{e_l} = \left[\frac{(\lambda + 2\mu)}{(\lambda_m + 2\mu_m)} (\xi + r_i)^2 N_i^{e_l} \frac{\partial \overline{u}^{e_l}}{\partial \xi} \right]_0^h \tag{7.33}$$

$$G_i^{e_l} = \left[\left\{ \frac{K}{K_m} \left(\delta_{2z} + s\delta_{1z} \right) + \frac{K^*}{a_0} \left(1 + \tau_1 s + z_1 \frac{\tau_1^2 s^2}{2} \right) \right\} \left(\xi + r_i \right)^2 N_i^{e_l} \frac{\partial \overline{\theta}^{e_l}}{\partial \xi} \right]_0^h \tag{7.34}$$

where, $i, j = 1, 2, ..., d$.

After assembling the element matrices given in the Eqn.(7.28) for all the elements, we get a system of $dM+d$ number of linear algebraic equations in unknown nodal values of displacement and temperature. While assembling, we interchange the rows and columns of element matrix so that the terms in the right hand sides of the Eqns. (7.26) and (7.27) canceled out by each other between any two adjacent elements, except the first node of the first element and last node of the last element. Further in-canceled terms of the right side of Eqns.(7.26) and (7.27) are known and related to the inner and outer boundary conditions as given by the Eqn.(7.22).

After using Eqns. (7.17) and (7.22) we get,

$$\overline{\theta}_1^{e_1} = \frac{\theta^*}{s}, \quad -a \left(\lambda_c + 2\mu_c \right) \frac{\partial \overline{u}^{e_1}}{\partial \xi}|_1 = \lambda_c \overline{U}_1^{e_1} - \frac{a \left(\lambda_m + 2\mu_m \right) \gamma_c}{\gamma_m} \overline{\theta}_1^{e_1} \tag{7.35}$$

$$\frac{\partial \overline{\theta}^{e_M}}{\partial \xi}|_d = 0, \quad \overline{U}_d^{e_M} = 0 \tag{7.36}$$

Further, using Eqn. (7.22), we obtain

$$\frac{\partial \overline{\theta}^{e_1}}{\partial \xi}|_1 = 0, \text{ and } \frac{\partial \overline{u}^{e_M}}{\partial \xi}|_d = 0 \tag{7.37}$$

Therefore, the sub-matrices of the global force matrix $\begin{bmatrix} [F] \\ [G] \end{bmatrix}$ are given by

$$[F] = \begin{bmatrix} \lambda_c \overline{U}_1^{e_1} - \frac{a(\lambda_m+2\mu_m)\gamma_c}{\gamma_m}\overline{\theta}_1^{e_1} \\ 0 \\ \vdots \\ 0 \end{bmatrix}, \quad \text{and} \quad [G] = \begin{bmatrix} 0 \\ 0 \\ \vdots \\ 0 \end{bmatrix} \tag{7.38}$$

Now, in obtained system of algebraic equations, $\overline{\theta}_1^{e_1}$and $\overline{u}_d^{e_M}$are known to us. Therefore, two rows and two columns intersecting the nodal values $\overline{\theta}_1^{e_1}$and $\overline{u}_d^{e_M}$ are deleted from the global stiffness matrix. At the same time in global force matrix $\begin{bmatrix} [F] \\ [G] \end{bmatrix}$, the sub-matrices will turn accordingly.

Therefore, all the unknown nodal values of displacement and temperature in (r, s) domain can be obtained by solving the updated linear system of algebraic equations given by Eqn. (7.28). To get the final solution in space-time domain, we employ the numerical method of Laplace inversion proposed by Zakian *et al.* (1969) for the better accuracy, since this method uses the complex numbers as nodes and weights for numerical integration appeared in the inverse of Laplace transform. The outline of the method has been provided in the Appendix section (A-2). We apply the second order finite difference scheme to get the solution for the stress components using the Eqns. (7.18)-(7.19).

7.4 Numerical Results and Discussion

In the previous section, we formulated finite element modeling of the present problem and obtained a system of linear algebraic equations. Now, in this section we carry out our computational work by using MATLAB program-

ming and obtain numerical solution of the present problem.We aim to analyze the effect of non-homogeneity of the material (non-homogeneity index n), time and relaxation parameters, τ, and τ_0 on distributions of displacement, temperature and stresses inside the spherical shell.The spherical shell is supposed to be initially at reference temperature, $T_0 = 298$K.Titanium and Zirconia are used for the metal and ceramic constituents for the functionally graded material. Therefore, the inner radius ($r_a = 1$) and outer radius ($r_b = 3$) of the shell are made of Titanium and Zirconia, whose physical properties are taken in SI units as follows (Bahtui and Eslami, 2007a):

Thermoelastic constants for the Titanium**:**

$E_m = 66.2$ GPa, $\alpha_m = 10.3\times10^{-6}$ K^{-1}, $c_{Em} = 808.3$ JKg^{-1}K^{-1}, $\rho_m = 4410$ Kg m^{-3}, $K_m = 18.1$ K^{-1}s^{-1}, $\nu_m = 0.321$.

Thermoelastic constants for the Zirconia**:**

$E_c = 117.0$ GPa, $\alpha_c = 7.11 \times 10^{-6}$ K^{-1}, $c_{Ec} = 615.6$ JKg^{-1}K^{-1}, $\rho_c = 5600$ Kg m^{-3}, $K_c = 2.036$ K^{-1}s^{-1}, $\nu_c = 0.333$.

The value of phase-lag parameters are taken as $\tau_0 = 0.1$, $\tau = 0.1$.

The formulation of the present set up is made for the general problem. However, in our computation, we use the linear Lagrangian polynomials as the shape functions in the base element. We break the shape of the spherical shell into $M = 100$ elements along the radius of the shell.Each element (e_l) is divided into $d = 2$ nodes. The displacement, u and temperature, θ in the space and Laplace transform domain, (r, s) are obtained by solving the system of Eqns. given by (7.28). The stresses in the (r, s) domain are computed by employing second order finite difference scheme from Eqns. (7.18) and (7.19) and by using the computed values of displacement and temper-

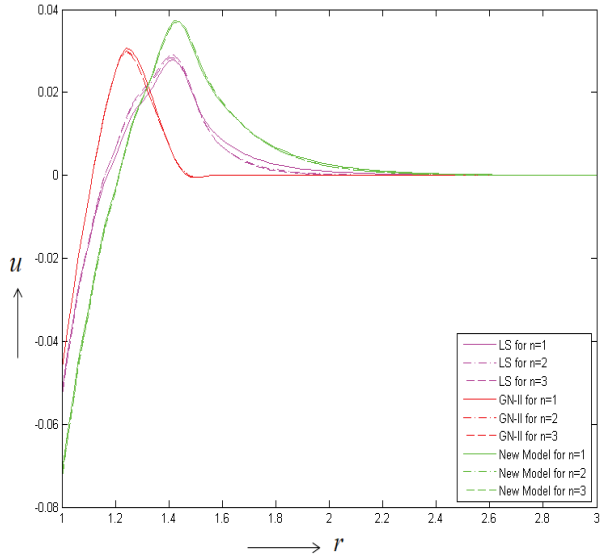

Figure 7.3: Variation of displacement, u vs. r at $t = 0.3$ for different values of n

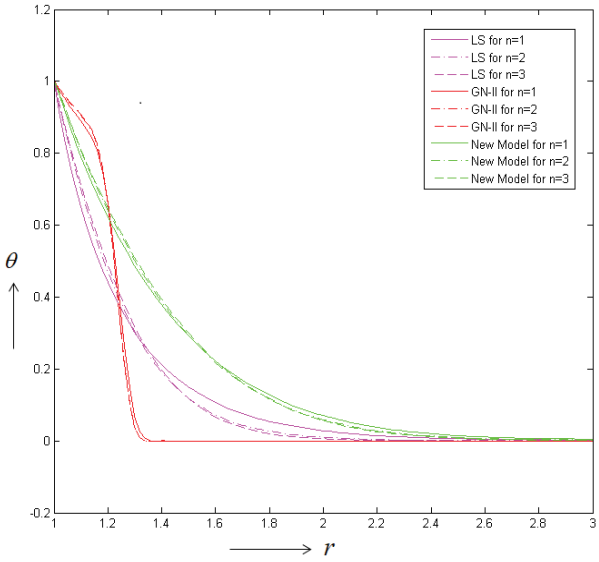

Figure 7.4: Variation of temperature, θ vs. r at $t = 0.3$ for different values of n

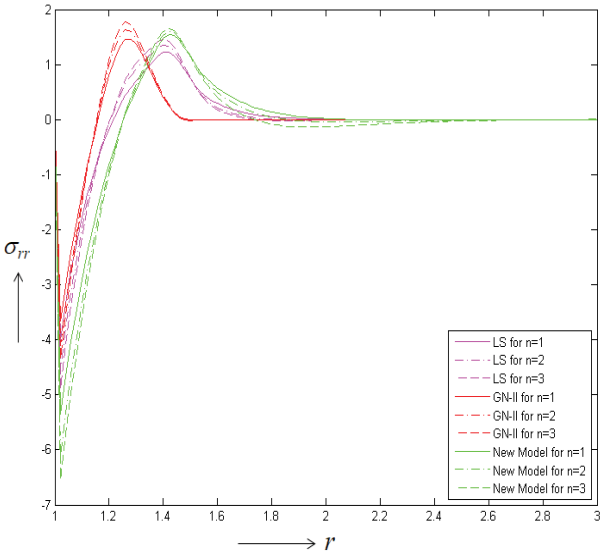

Figure 7.5: Variation of radial stress, σ_{rr} vs. r at $t = 0.3$ for different values of n

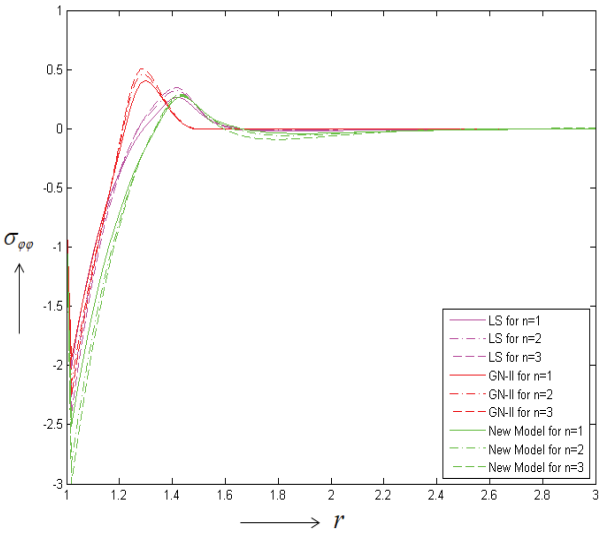

Figure 7.6: Variation of circumferrential stress, $\sigma_{\varphi\varphi}$ vs. r at $t = 0.3$ for different values of n

ature of (r, s) domain. Finally, we employ the Zakian technique (1969) for the numerical inversion of Laplace transform to obtain the desired field variables in space-time (r, t) domain.

All the calculations are carried out for three different values of non-homogeneity index, n ($n = 1, n = 2$ and $n = 3$).

The obtained results for displacement (u), temperature (θ), radial stress $(\sigma_{rr)}$ and tangential stress $(\sigma_{\varphi\varphi)}$ for LS model, GN-II model and New model are shown by different 2D and 3D plots. The 2D[2] representation of displacement, temperature, radial stress and tangential stress are displayed in the Figs. (7.3-7.6), respectively for a fixed time, $t = 0.3$ to show the effect of non-homogeneity index on the distributions of different physical fields predicted by different models. The 3D graphs are shown in the Figs. $7.7(a, b, c)$-$7.10(a, b, c)$ to characterize the the effect of time, t on the field variables. The 3D plots in the Figures sketched in magenta color (Figs.$7.7(a)$, $7.8(a)$, $7.9(a)$, and $7.10(a)$) display the variation of different field variables predicted by LS model. The Figures sketched in red color (Figs.$7.7(b)$, $7.8(b)$, $7.9(b)$, and $7.10(b)$) represent the variation of the fields predicted by GN-II model, and the Figures sketched in green color (Figs.$7.7(c)$, $7.8(c)$, $7.9(c)$, and $7.10(c)$) show the variation of the fields predicted by New model (Quintanilla model, 2011). In all the Figs. ($7.7(a, b, c)$-$7.10(a, b, c)$), we take the non-homogeneity index, $n = 2$.

Fig.(7.3) and Figs. $7.7(a, b, c)$ show the variation of displacement, u under different models at different time. Fig.(7.3) indicates that the predictions by different models are significantly different. At any particular time,

[2]Note: In the 2D plots, variation of filed variables is shown up to $r = 2$, since the field variables vanish beyond $r = 2$.

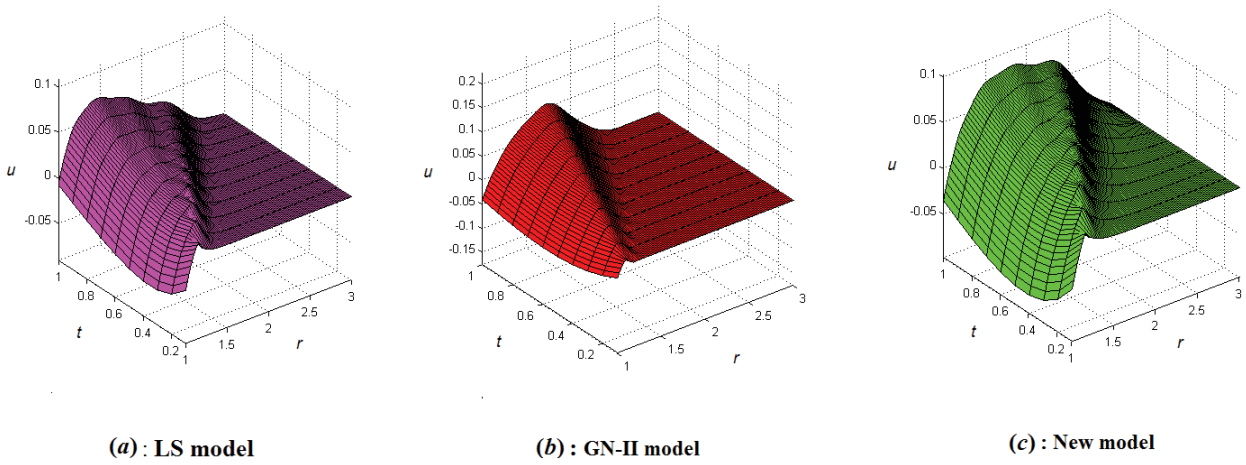

Figure 7.7: ***(a,b,c).*** Variation of displacement, u for different values of r and t and for $n = 2$

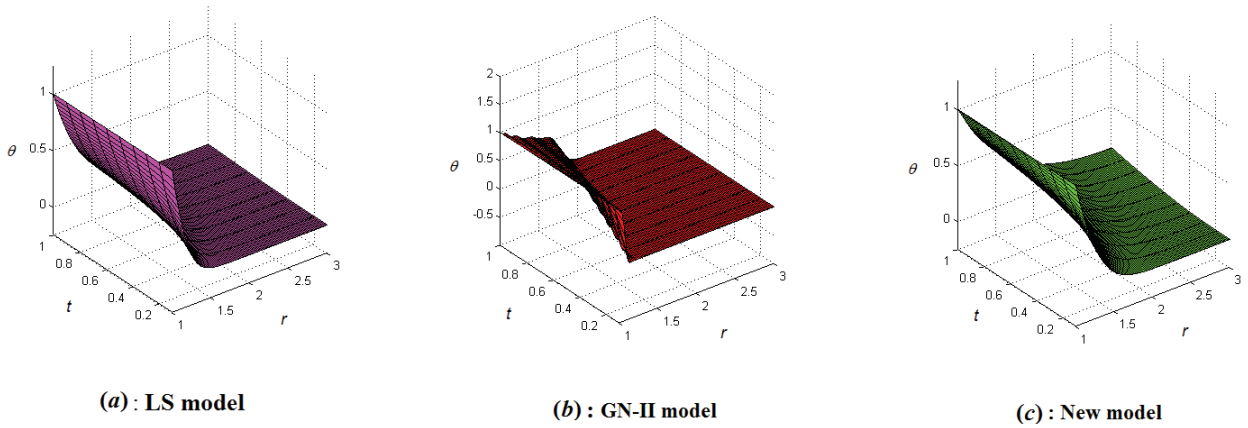

Figure 7.8: ***(a,b,c).***Variation of temperature, θ for different value of r and t and for $n = 2$

the numerical values of displacement is maximum in case of New model and is minimum in case of LS model. Further, it is concluded from the Fig.(7.3) that displacement is directly proportional to the non-homogeneity index, n for a particular model. Also as the radial distance, r gets closer to the radius of outer boundary of the shell, the displacement becomes zero which is in agreement with the boundary condition prescribed for the displacement. For a fixed time, t, the displacement starts increasing from the radius of inner boundary of the shell and after getting a maximum value, it tends to zero values in all cases. The Figs.7.7(a, b, c) characterize the displacement with the variation in time for a particular value of the non-homogeneity index, n. We consider the case when $n = 2$. It shows that as time increases, the maximum peak in displacement shifts in the increasing direction of r. Further, the displacement gets zero after traveling less distance at lower time and it travels larger distance to get zero value as time increases for each and every model. The region of influence inside the shell is minimum in case of GN-II model and it is maximum in case of New model. The region of influence increases with time in the context of each model.

Fig. (7.4) indicates the behavior of temperature. It clearly reveals that the inner boundary condition given to the temperature (θ) is satisfied. We further note that there is significant disagreement in predictions by different models for temperature field too. The temperature for New model is higher as compared to the LS model, while GN-II model shows the highest value for temperature nearer the inner boundary of the shell and gets lowest value after traveling some radial distance, r as compared to the other two models. The temperature field achieves higher values for larger value of

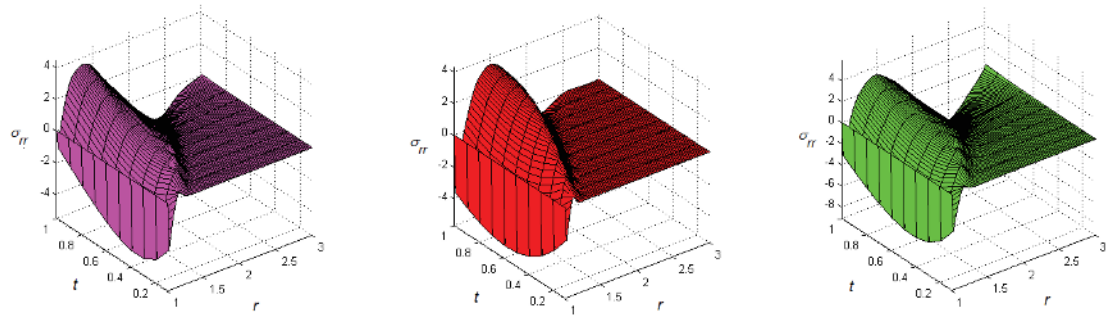

Figure 7.9: ***(a,b,c).*** Variation of radial stress, σ_{rr} for different values of r and t and for $n = 2$

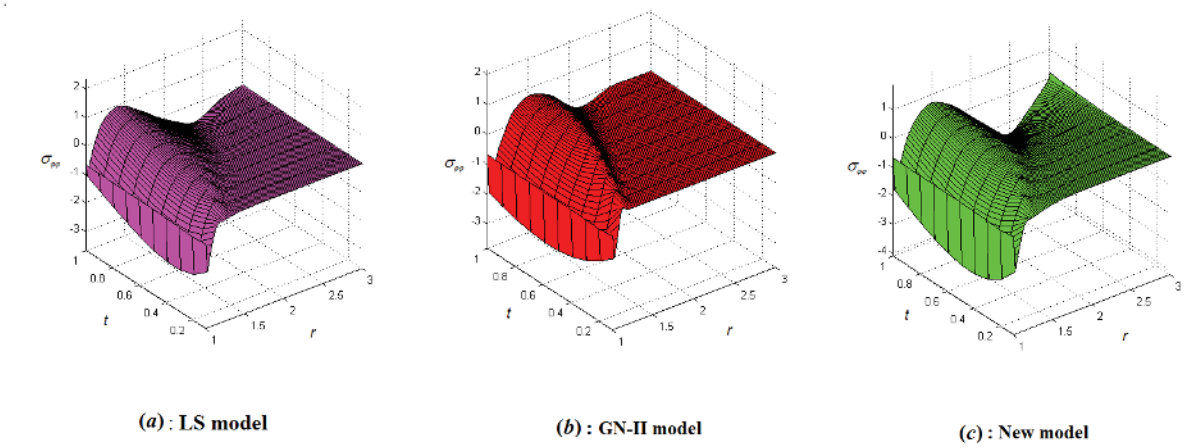

Figure 7.10: ***(a,b,c).***Variation of circumferential stress, $\sigma_{\varphi\varphi}$ for different value of r and t and for $n = 2$

non-homogeneity index n nearer to the inner boundary of the spherical shell, while after traveling some radial distance, it gets larger values for smaller values of n. GN-II theory predicts very small negative value for some small interval of radial distance, r as it is obvious from previous literature in the case of thermoelasticity theory for GN-II model. The temperature tends to zero as radial distance tends to the outer radius of the shell. Figs. $7.8(a, b, c)$ show more clearly the variation of temperature for different models at different times and for the case when $n = 2$. It is clear that at the larger time, the temperature travels till larger distance to get zero value under LS model and New model. However, it sharply tends to zero in case of GN-II as compared to the other models. This implies that at any time the region of influence for temperature is minimum in the context of GN-II model as compared to the other two models.

From the Figs. (7.5) and (7.6), it is evident that both the stresses are compressive in nature nearer to the inner boundary of the shell and radial stress σ_{rr} satisfies the inner boundary condition. Also it is evident that both the stresses show one local minimum and one local maximum in the context of each model. The effective region for both the stresses under three models shift along the right direction in the order as GN-II, LS and New model and local maximum also shifts in the same order. Further, the effect of non-homogeneity index, n is very much prominent on both the stresses σ_{rr} and $\sigma_{\varphi\varphi}$. Generally, the values of stresses increase for larger value of n but this result is in reverse order for some small interval of radial distance, r. Figs. $7.9(a, b, c)$ and $7.10(a, b, c)$ depict the 3D plots of stresses to characterize the effect at different time for a particular non-homogeneity

index. From these Figures, it is clear that at a larger time, t the stresses travel more radial distance to get zero values and the effective region of influence increases with time in case of each model.

7.5 Conclusions

We investigate a problem concerning thermoelastic interactions inside a medium with functionally graded material properties. Some important points of the present study can be demonstrated as follows. The spherical shell made with functionally graded materials is highly supported in modern design of engineering. Therefore, the thermoelastic investigation for such problems is very popular now. It considers realistic situation that takes into account the coupling effects of temperature and mechanical fields involved in the problem. The importance of finite element method to tackle the problem has been illustrated. Previously, Bellman method or Fourier series method or Stehfest method are used for Laplace inversion to get the final solution in space time domain. However, we employ here the method proposed by Zakian *et al.* (1969) for the better accuracy. FEM software packages like ANSYS, ABAQUS are commonly used in thermoelasticity theories but we give a detailed mathematical description of the finite element method to tackle the problem. We carry out our computation successfully. The present study also highlights the effects of employing the New heat conduction model proposed by Quintanilla (2011) over the cases of other two existing thermoelastic models. We observe that the predictions of different models are significantly different and the New model shows the highest disturbance range due to thermal loading as compared to

the other two models. The GN-II model has the lowest region of influence for each field at any time.